Dynamic Jahn-Teller Effect for Cr^{2+} in MgO: Hypersonic Attenuation*

James N. Lange
Department of Physics, Oklahoma State University, Stillwater, Oklahoma 74074
(Received 21 May 1973)

The acoustic attenuation due to scattering from Cr^{2+} substitutional impurities in MgO provides information on both the symmetry and energy of the states of the impurity system. Only acoustic modes which serve as a basis for an E irreducible representation are observed to be resonantly scattered by the Cr^{2+} impurity system. Assuming the states of the impurity and its nearest neighbors can be approximated to first order by a molecular cluster, the acoustic modes with E irreducible representation are the ones that excite the molecular-cluster vibrational mode which interacts with the electronic configuration and splits the degenerate ground state. The resonant scattering which leads to a relaxation maximum in the attenuation as a function of temperature, is interpreted as being due to indirect transitions. Energy-level separations, determined from the relaxation absorption, suggest a Jahn-Teller tunneling splitting of approximately 14 cm^{-1} (1.75 meV). A detailed comparison of the experimental energy-level separations determined from the hypersonic relaxation exhibits substantial agreement with the calculated energy levels of Fletcher and Stevens and is consistent with the thermal-conductivity measurement of Challis *et al.* A uniaxial stress leads to a splitting of the relaxation peak and when fitted to the stain-dependent theoretical calculations, yields a Jahn-Teller coupling energy of 8.1×10^{13} cm^{-1}/m in approximate agreement with the point-ion approximation.

I. INTRODUCTION

The presence of isolated substitutional impurities can substantially modify the lattice transport properties of a solid. This is particularly true of strong-coupling ions which distort the lattice locally and, by removing orbital degeneracies, exhibit a Jahn-Teller effect. These distortions are stabilized by the anharmonic components of the lattice displacements. Transitions between equivalent distorted configurations yields the dynamic Jahn-Teller effect. This latter effect is of particular interest in this investigation, which considers the interaction of lattice waves of well-defined polarization and mode type with the impurity system. The interaction of the acoustic wave with the impurity system results in a scattering of the acoustic energy and manifests itself as an attenuation of the acoustic wave. The attenuation due to scattering from the impurity system is in addition to the contribution from phonon interactions in the host lattice.

The substitutional impurity of interest in this investigation is the chromous ion (Cr^{2+}) embedded in a MgO host lattice. The chromous ion has a $3d^4\ {}^5D_0$ configuration which leads to an E_g^e ground state [the superscript e indicates an irreducible representation (i.r.) for the electronic configuration, while a superscript v indicates an i.r. for a vibrational mode] in the cubic field (O_h) of the MgO. The E_g^e ground state provides a system in which vibrational-electronic interactions are particularly obvious, since the spin-orbit interactions are suppressed in the cubic field. The second-order contribution of the spin-orbit interaction is apparent since the product of the i.r. of the ground state ($E_g^e \times E_g^e = A_{1g}^e + A_{2g}^e + E_g^e$) does not contain the i.r. of the angular momentum components (T_{1g}).

Since the chromous ion is tightly bound to the nearest neighbors, a molecular-cluster model is employed to interpret the experimental results. The molecular cluster is octahedrally coordinated and consists of the chromous ion and its six-nearest-neighbor oxygens. The molecular cluster is embedded in the host lattice which interacts through scalar coupling with the lattice background. This model is proposed by Bates, Dixon, Fletcher, and Stevens[1] in the treatment of ion-lattice interactions of E_g-type ions. The particular case of the chromous ion in MgO has been treated theoretically by Fletcher and Stevens[2] using this model and independently by Ham[3] to explain the acoustic-paramagnetic-resonance (APR) data of Marshall and Rampton.[4]

The states of the molecular cluster depend on coupling of the electronic configurations and the vibrational modes of the cluster. The interaction between the various vibrational normal modes of the cluster and the electronic states is critically dependent on the symmetry. In this investigation, only the electronic ground state is of interest, for the first-excited state is far above [> 16 000 cm^{-1} (2×10^3 meV)] any excitations available. Since the electronic ground state is a basis for an E_g^e i.r., only vibrational modes which have i.r. within the product $E_g^e \times E_g^e = A_{1g} + A_{2g} + E_g$ will interact. The isolated octahedral molecular cluster has normal modes[5] which are the basis for $A_{1g}^v + E_g^v + 2T_{1u}^v + T_{2g}^v + T_{2u}^v$ i.r., but only the A_{1g}^v and E_g^v are members of the orbital product and interact with the

electronic ground state. The normal-mode displacements for the singlet A_{1g}^{v} and doublet E_{g}^{v} are shown in Fig. 1.

Embedding the molecular cluster in the host lattice provides a means of interaction of the lattice modes with the vibrational-electronic system. If the coupling between the lattice and cluster depends only on the relative displacements of the molecular cluster and the lattice, the coupling will be scalar (A_{1g}). Thus, only lattice modes which are a basis for A_{1g}^{L} and E_{g}^{L} configurations will interact with the vibrational-electronic states of the molecular cluster. This leads to a selectivity as to which acoustic modes will be effected by scattering from the molecular cluster. Only acoustic modes containing the E_g representation are observed to exhibit the acoustic-relaxation phenomenon associated with resonance scattering from the molecular cluster.

As first proposed by Jahn and Teller, the electronic ground-state (E_g) degeneracy is removed by interaction with the vibrational modes. The separation of the former degenerate electronic states is approximately 1400 cm^{-1}. In this investigation, excitations of energies of considerably less than 100 cm^{-1} are considered and thus, only the lower levels of the split electronic ground state is of interest.

To stabilize the Jahn-Teller distortion in the cubic field of the lattice, higher-order anharmonic terms must be included in the vibrational Hamiltonian. The strength of the anharmonic terms will be referred to as B, following the notation of Fletcher and Stevens. The anharmonic terms introduce a potential barrier which stabilizes the Jahn-Teller distortion in either of three equivalent positions along the fourfold axes of the octahedron. Tunneling between equivalent configurations leads to the dynamic Jahn-Teller effect and the so-called "inversion splitting." The tunneling splitting δ is dependent on the height of the barrier which, in turn, is dependent on the magnitude of the parameter B. The sign of B determines whether the distortion is a compression along one of the fourfold axes ($B>0$) or an elongation ($B<0$). The behavior of the lowest Jahn-Teller energy level is shown in Fig. 2 for various values of B indicating the tunneling splitting δ. When $|B| \to \infty$, the tunneling splitting is zero, and the energy level diagram is that of an anharmonic oscillator. The tunneling splitting is of particular interest in this investigation in which the acoustic wave is scattered by the molecular cluster. The resonance

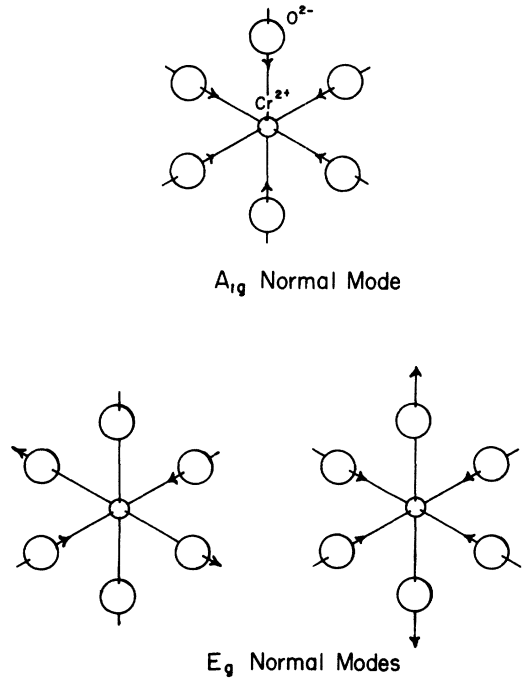

FIG. 1. Displacements of the A_{1g}^{v} and E_{g}^{v} normal modes for an octahedral molecule consisting of a chromous ion and six oxygens.

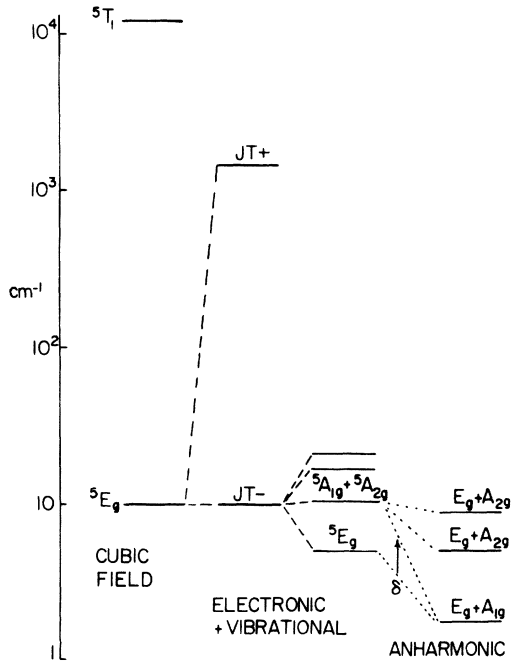

FIG. 2. Representative energy-level diagram for the chromous ion in a cubic field. The ground-state degeneracy is removed by interaction with vibrational modes into Jahn-Teller states (JT+ and JT−) which are stabilized by anharmonic effects. The magnitude of the anharmonic effects determine the tunneling splitting δ ($E_g \to A_{1g}$). For increasing anharmonic effects the level separations approach those of a harmonic oscillator and the tunneling splitting goes to zero (the E_g and A levels coalesce).

scattering corresponds to the acoustic period equal to the transition rate between these sets of levels. From the acoustic measurements, information concerning the magnitude of the tunneling splitting is obtained.

The energy level diagram of Fig. 2 is not complete, since it does not reflect the spin-orbit interaction. Although the spin-orbit interaction is second order compared to the vibrational-electronic terms, it is significant in resolving the ground-state vibrational-electronic levels to better than 20 cm^{-1}, as is possible with acoustic measurements at low temperatures. The spin-orbit interaction further reduces the tenfold degeneracy of the tunnel split levels, and will be treated in more detail in a later section.

EXPERIMENTAL PROCEDURE

The elastic properties of crystalline solids are quite anisotropic reflecting the symmetry of the lattice. In general, energy propagation of a stress wave does not occur along the same direction as the wave vector. There are, however, particular directions in a crystalline solid for which the direction of the energy transport and wave vector are parallel. The displacements of waves propagating along these directions can be decomposed into either longitudinal or transverse modes which propagate with characteristic velocities. These particular directions are often along high-symmetry directions of the lattice and will be referred to as pure mode directions. Propagation of stress waves along these pure mode directions leads to a unique characterization of the polarization, wave vector, and mode type even on an atomic scale.

The particular mode of interest can be generated preferentially by piezoelectric material which is oriented to provide either a longitudinal or transverse strain. The transducer (usually quartz) is bonded to a flat polished surface of the crystal which is perpendicular to the direction of propagation. The alternating strain propagates into the crystalline solid to a second parallel face approximately 2 cm from the first. The stress wave is reflected and returns to the piezoelectric material, which now acts as a receiver and converts a small part of the acoustic energy to an electrical signal. A tunable microwave cavity couples this energy into a heterodyning receiving system. The propagation of the stress wave pluse is displayed as a series of echos whose separation is inversely proportional to the velocity of the pure mode and whose amplitude is inversely proportional to its attenuation (Fig. 3). The amplitude of the pulse decreases as a result of the scattering of the acoustic energy from the propagating media. To facilitate the determination of the attenuation coefficient, the exponential decrease in pulse height is operated on by a logarithmic amplifier resulting in a linear

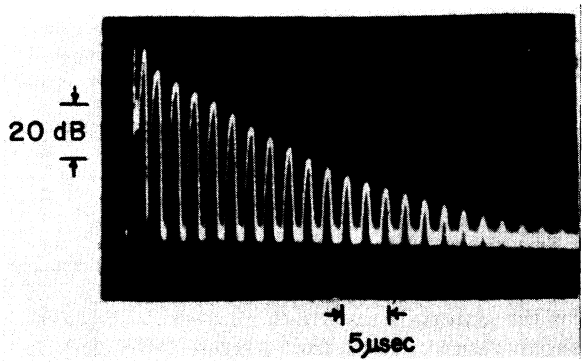

FIG. 3. Echo pattern for a longitudinal pulse which is multiply reflected between two parallel faces of sample No. 2. The pulse is propagating along the [100] direction at 77 °K. Logarithmic amplification leads to the linear decrease in amplitude of the pulse envelopes. The carrier frequency (1 GHz) has been heterodyned and processed by a video detector.

decay of the pulse height over much of its range. The pulse duration is long enough so that the Fourier spectrum is localized around the carrier frequency. The attenuation is then assumed to be dominated by the carrier frequency and closely approximates the behavior of a monochromatic wave. Typically, pulses consisting of a thousand cycles with a carrier frequency of 1–3 GHz are used.

The attenuation of the acoustic wave can be considered as consisting of two components, one being due to phonon interactions in the host MgO lattice while the other is due to dynamic effects associated with impurities. This latter component is the primary concern of this investigation; however, the attenuation of the host MgO lattice will be considered first. The attenuation of acoustic waves in insulators typically consists of a constant low-temperature (< 10 °K) component and a power-law increase in attenuation at intermediate temperatures ($10 < T < 100$ °K). The constant low-temperature background is attributed to scattering by impurities and imperfections which leads to a constant acoustic-phonon mean free path. This scattering does not exhibit the dynamic features which are to be considered in detail later but is analogous to the Mathiesen region of low-temperature resistivity. The frequency dependence of the attenuation for various modes is shown in Table I.

The attenuation in the intermediate temperature range usually exhibits a T^n dependence, where n depends on the type of mode. The exponent for various pure modes is listed in Table II. The magnitude of the exponent exhibits considerably less variation from mode to mode than has been observed in other insulators.[6]

The host crystals of MgO contain a variety of low-concentration substitutional impurities which,

TABLE I. Low-temperature (1.2 °K) frequency dependence of the attenuation coefficient ($\alpha = b\omega^m$) between 1 and 3 GHz. The specimen is prepared so that no relaxation is observed.

Propagation direction	Polarization	m
Longitudinal [100]	[100]	1.2
Longitudinal [110]	[110]	1.5
Transverse [100]	[010]	−1

for the materials used in this investigation, are summarized in Table III.[7] A systematic study is necessary to determine the specific origin of the acoustic attenuation. This study is facilitated by the fact that the valence of some of the impurities can be changed by γ irradiation without introducing lattice damage.[8] Many of the transition-metal impurities substantially change their coupling to the lattice with changes in valence. The valence state of many of the paramagnetic impurities can be determined from electron-paramagnetic-resonance (EPR) data. The magnitudes of the EPR signals are used to determine the relative magnitudes of the paramagnetic impurities in a particular valence state. The occupancy of valence states which are too strongly coupled to the lattice to be observed at 77 °K by EPR are implied from the number in a complimentary state. The number of impurities in a particular valence state is correlated with the magnitude of the acoustic relaxation absorption as a function of various thermal and irradiative treatments. As can be seen from Fig. 4, the relaxation absorption varies in magnitude of the Cr^{2+} impurities.

To determine whether this agreement is fortuitous and the maximum in attenuation is due to a valence change of a nonparamagnetic impurity, a series of samples of varying impurity concentrations are investigated. An example of the relaxation maximum for two samples of similar nonparamagnetic impurity concentrations (but Cr^{2+} concentration varying by a *factor* of 10) is shown in Fig. 5. The magnitude of the relaxation is seen to scale linearly with the relative magnitudes of the Cr^{2+} concentrations and not with the nonparamagnetic impurity concentration. Thus, the relaxation maximum is assumed in the following to be due to Cr^{2+} substitutional impurities.

TABLE II. Exponent of the temperature dependence of the low-temperature attenuation ($\alpha = aT^n$) for various modes and polarizations at 1 GHz. The specimen is prepared so that no relaxation is observed ($10 < T < 100$ °K).

Propagation direction	Polarization	Stiffness modulus	n
Longitudinal [100]	[100]	C_{11}	3
Longitudinal [110]	[110]	$\frac{1}{2}(C_{11}+C_{12}+2C_{44})$	3
Transverse [100]	[010]	C_{44}	1.5
Transverse [110]	[$\bar{1}$10]	$\frac{1}{2}(C_{11}-C_{12})$	3
Transverse [110]	[100]	C_{44}	<1

TABLE III. Paramagnetic impurity concentration in parts per million for MgO specimens.

Specimen	Fe	Cr	Mn	V
No. 1	3	2	1	<5
No. 2	70	21	9.4	

MOLECULAR SCATTERING AND ACOUSTIC RELAXATION

The strong coupling of the chromous ion to the lattice suggests a description of its dynamic properties in terms of a molecular cluster formed by the chromous ion and its nearest neighbors. The molecular cluster is then made up of the chromous and six octahedrally coordinated oxygen ions. The molecular cluster is coupled to the perfect host lattice in a manner which does not substantially perturb the states of the cluster. To first order,

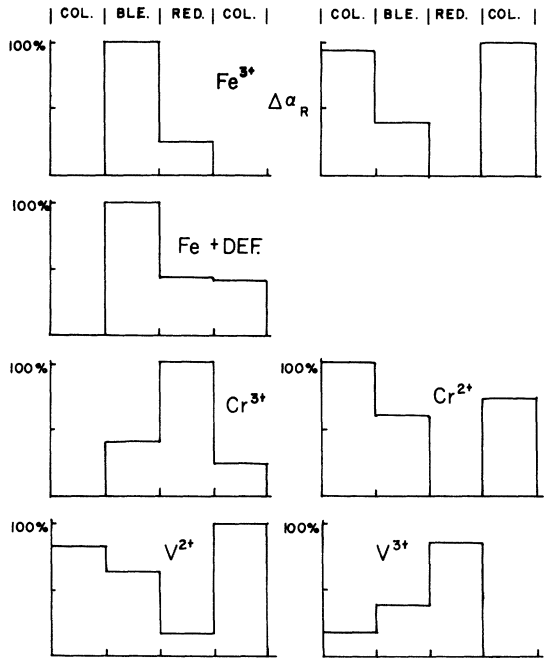

FIG. 4. First column of figures displays the magnitude of the EPR signal for paramagnetic impurities in specimen No. 1 as a function of various thermal and irradiative treatments. The second column indicates the changes in complimentary valence states deduced from the first column and assuming the impurity concentration is constant. The magnitude of the relaxation is indicated by $\Delta\alpha_R$ which is the maximum attenuation. The abbreviation COL. refers to introducing color centers (primariiy V centers) through γ irradiation in a ^{60}Co-γ cell, while BLE. refers to heating to 100 °C to bleach the color centers and RED. refers to vacuum reduction at 1100 °C in the presence of a Ti getter. The magnitude of the relaxation correlates with the number of chrome ions in the 2+ state.

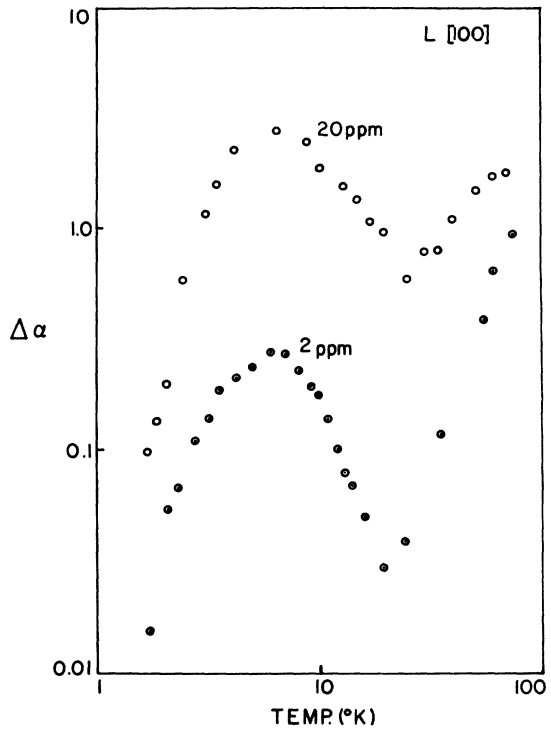

FIG. 5. Relaxation absorption of a longitudinal mode propagating along the [100] in specimen No. 1 (⊙) and specimen No. 2 (○). The factor-of-10 increase in chromium impurities results in a factor-of-10 increase in the magnitude of the relaxation maximum even though the nonparamagnetic impurities are approximately the same for both specimens. As will be the case for most of the ensuing figures, the ordinate is the logarithm of the attenuation with the abscissa being the logarithm of the temperature (1 GHz).

then, the impurity is part of an octahedral molecule which is coupled to the host lattice. The attenuation of the acoustic wave results from scattering of the stress-wave energy from the molecular cluster. It is apparent that the stress wave does not induce any direct transitions in the molecular cluster by single phonon inelastic events as the phonon energies of the stress wave (< 0.08 cm^{-1}) are considerably less than the energy-level separations.

The scattering of the stress wave is also not a simple Rayleigh scattering, since the molecular cluster is continually changing state. The cluster is excited or pumped by the thermal phonon sea through the resonant absorption (direct transitions) and Raman scattering. The lifetime of the cluster in any state is proportional to the transition probability times the number of thermal phonons with energies greater than the level separation (~ 20 cm^{-1}). The lifetime is temperature dependent and reflects the change in the occupancy of the thermal phonons as the temperature changes. The molecular cluster can thus be viewed as a dynamic scattering center which is making transitions between states at a rate proportional to the occupancy of the thermal phonon density of states. When the stress-wave frequency is synchronized with the transition rate, a maximum scattering of the stress wave occurs which in turn leads to a maximum in acoustic attenuation.

The scattering of the stress wave is strictly speaking a Raman process but because the wavelength of the stress wave is much larger than both the molecular cluster and the dominant thermal phonon, it is more intuitive to consider it as a classical resonance scattering rather than the virtual absorption and readmission associated with the Raman process. In contrast, the thermal-phonon scattering by the molecular cluster can be conveniently characterized by Raman and direct processes. The scattering of the stress wave by the molecular cluster is depicted in Fig. 6. The attenuation of the stress wave results primarily from acoustic energy being scattered from the initial beam.

The magnitude of the relaxation process varies with the stress wave frequency, with the attenuation coefficient α being directly proportional to the frequency (Fig. 7). This indicates that for a dispersionless material, the attenuation per cycle of the stress wave is constant. The molecular cluster acts as a scattering center whose dynamics are not appreciably affected by the acoustic wave, which acts as a small perturbation. The scatter-

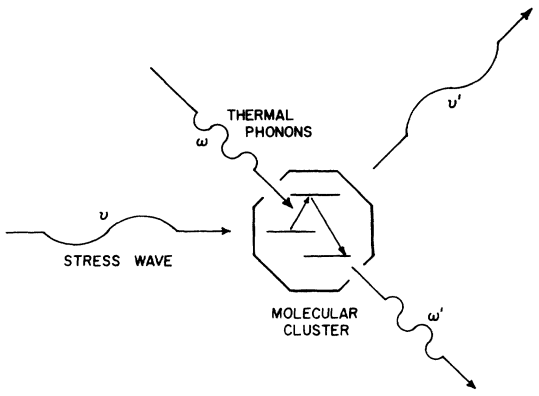

FIG. 6. Stress wave of frequency ν is scattered by the molecular cluster out of the primary sound beam leading to an attenuation of the phase and geometrically correlated sound beam. The molecular cluster is excited by thermal phonons (ω) with a transition rate $1/\tau$. Resonant scattering occurs when $\nu\tau = 1$. The wavelength of the stress wave ($< 10^4$ Å) is considerably larger than the molecular cluster and leads to a constant scattering per cycle for the low-frequency stress waves ($\nu \ll \omega$).

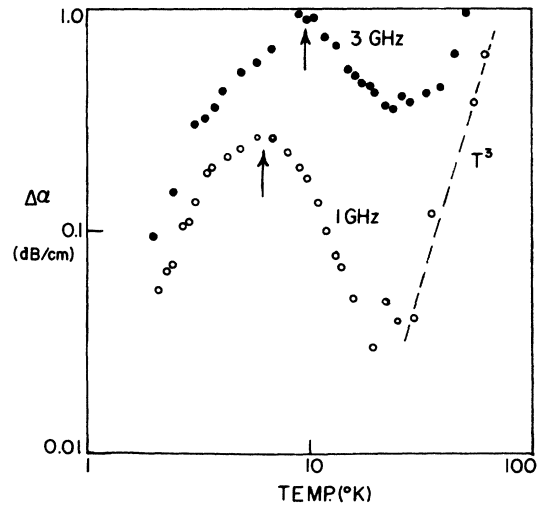

FIG. 7. Attenuation coefficient of a longitudinal mode propagating along the [100] direction in specimen No. 1. The maximum in attenuation occurs at 6.5 °K for an acoustic frequency of 1 GHz (O) and at 10 °K for a frequency of 3 GHz (●). The maximum in attenuation corresponds to a transition rate equal to the period of the wave $\nu\tau = 1$.

ing cross section at resonance ($\nu\tau = 1$) remains constant so that the energy scattering per cycle is independent of frequency. The dynamics of the cluster reflect the transitions due to the thermal-phonon sea. The scattering strength near resonance is primarily a temporal rather than a geometric affect.

The transition rate of the excitations of the molecular cluster changes with temperature proportional to the occupancy of the thermal-phonon density of states. In the measurements reported in this invesitgation, the frequency of the stress wave is fixed and the temperature is varied over a range in which the transition rate approaches the frequency of the stress wave. The attenuation of the stress wave goes through a maximum at some temperature T_m when the transition rate $(1/\tau)$ is equal to the frequency of the stress waves ν such that $\nu\tau(T_m) = 1$. As can be seen in Fig. 6 as the stress-wave frequency is increased, the temperature at which this attenuation maximum occurs also increases.

Two types of transitions between the vibrational-electronic states of the molecular cluster are likely to be induced by the thermal phonons. The first is direct transitions between pairs of energy levels of the system while the second is an indirect transition between multiple levels of the cluster. The indirect or Orbach process[9] is consistent with the observed temperature dependence of the relaxation maximum and is assumed to be the dominant process monitored by the stress wave. The transition rate for indirect transitions is given by

$$1/\tau = (1/\tau_0)e^{-\Delta/kT}, \tag{1}$$

where Δ is the separation between two levels $A \rightarrow B$ and $1/\tau$ the transition rate for the entire process $A \rightarrow B \rightarrow C$. The indirect transition is not only consistent with the temperature dependence of the relaxation maximum, but also with the selection rules for a proposed energy level scheme considered in a later section.

When Eq. (1) is combined with the resonant scattering condition $\nu\tau = 1$, a quantitative determination of τ_0 and the energy level separation Δ can be made. Measurements of the temperature of the relaxation maximum at two different frequencies leads to a unique determination of the parameters τ_0 and Δ. From the information contained in Fig. 7, the energy level separation is found to be $\Delta = 14\ \text{cm}^{-1}$, while the prefactor $\tau_0 = 4 \times 10^{-11}$ sec. The energy-level separation Δ is consistent with the energy-level diagram of Challis *et al.*[10] necessary to explain resonant scattering in the thermal conductivity. The energy separation is proportional to the Jahn-Teller inversions or tunneling splitting between the ground state E and excited A_1 or A_2 levels and will be considered in more detail in a later section.

The prefactor τ_0 is the asymptotic value of the transition rate at high temperatures. The value determined from the relaxation measurements indicates the transitions are between levels which are allowed to first order. Thus, in identifying transitions which might be involved in the relaxation scattering, only sets of levels separated by $\sim 14\ \text{cm}^{-1}$ which are allowed by the selection rules will be considered.

SYMMETRY CONSIDERATION

Propagation of lattice waves in crystalline solids is quite anisotropic and only along particular directions in the crystal can waves be characterized as either transverse or longitudinal. The polarizations for the two independent transverse and one longitudinal mode form an orthogonal triad along the pure-mode directions and maintain their particular polarization as they propagate with a characteristic velocity. The displacements of the pure modes can be related in a simple way to atomic displacements of the lattice. Thus, the interaction of these pure modes with impurities such as the chromous molecular cluster can be related to the symmetry of the displacements of the pure modes and the symmetry of the states of the molecular cluster. In the following, we will consider the stress wave as propagating in a perfect lattice until it encouters the molecular cluster and is partially scattered by it. The coupling between the perfect lattice and the molecular cluster

is assumed to be scalar and not significant in reducing the symmetry of the interaction between the cluster and the stress wave. The impurity concentration is low so isolated scattering without any direct interaction between clusters is most likely.

To characterize the interaction of the pure-mode stress wave with the molecular cluster, the techniques of group theory are used. Pure modes with the same polarization and propagating along equivalent directions in the crystal serve as basis functions to determine their irreducible representations under the operations of the cubic group (O_h). The genesis of this approach was developed by Nowick and Heller for stress induced rigid reorientation of impurities. In this work we are particularly concerned with internal modes of the molecular cluster and not rigid reorientation as were Nowich and Heller.[11] As a boundary condition we must keep in mind that stress waves are centrosymmetric and therefore possess only even (or gerade) irreducible representations. The stress-strain relationships only consider displacements which can be generated by forces applied to unconstrained boundaries which do not lead to a displacement of, or rotation about, the center of mass.

The coupling of the stress wave to the molecular cluster is scalar or through an A_{1g} representation. Because of the simplicity of the coupling the irreducible representations of the stress wave are coupled directly to the irreducible representations of the molecular cluster. Another way of expressing the coupling condition is that the product of the irreducible representations of the stress waves with the irreducible representation of the coupling reproduces only the irreducible representations of the stress wave.

As an example of the selectivity of the stress wave in defining the dynamic symmetry of the molecular cluster let us consider the transverse modes which propagate along the [110] direction (face diagonal) in a cubic crystal. The two orthogonal polarizations of the stress wave propagate with different velocities. The polarizations of these two modes is in the [001] direction (fast-transverse mode) or the [110] direction (slow-transverse mode) with their stiffness constants given in Table IV. The irreducible representations for these two modes are also listed in Table IV, and can be seen to be quite distinct. Pure modes

TABLE IV. Irreducible representations for a basis consisting of equivalent transverse modes propagating in a cubic lattice.

Mode	Stiffness constant	Irreducible representation
Slow transverse	C_{44}	$T_{1g} + T_{2g}$
Fast transverse	$\frac{1}{2}(C_{11} - C_{12})$	$A_{1g} + E_g + T_{1g}$

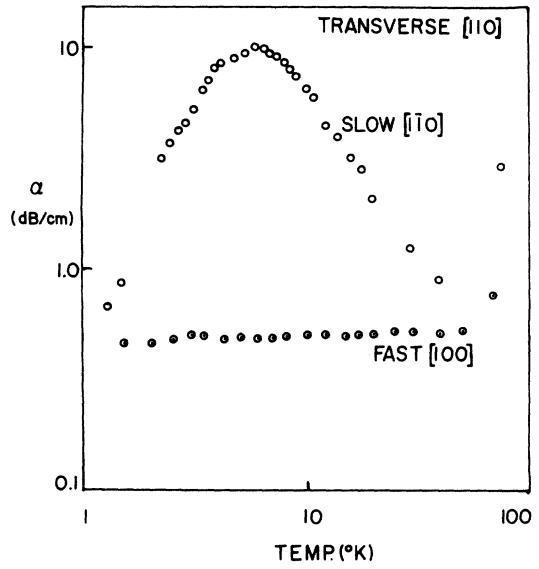

FIG. 8. Attenuation coefficient of two transverse modes propagating along the [110] direction in specimen No. 1. The transverse polarization for the fast mode is in the [100] (fast, ⊙) and for the slow mode in the [1$\bar{1}$0] (slow, O) direction. The relaxation absorption is exhibited by the slow-transverse mode which is a basis for an E_g^v i.r. but not for the fast-transverse mode (T_{2g} i.r.) (1 GHz).

in other directions always contain a mixture of these two i.r. The slow-transverse mode is a basis for an E_g i.r., while the fast-transverse mode is a basis for a T_{2g} i.r. for the cubic group.

The observed attenuation of these pure modes reflects their difference in symmetry as can be readily seen in Fig. 8. The relaxation maximum is present for the slow-transverse modes at the same temperature as observed for the longitudinal modes of Fig. 6. There is no relaxation observed for the fast-transverse mode along this and all equivalent directions in the crystal. This observation coupled with measurements on longitudinal modes indicates the interaction with the molecular cluster is with states that possess the E_g i.r. (Table V).

These observations are consistent with matching the acoustic i.r. with the i.r. of the vibrational mode of the octahedral molecule which interacts with the electronic ground state. The interaction of the E_g^v vibrational mode with the electronic ground state is responsible for the lifting of the orbital degeneracy of the E_g^e ground state. The T_1^v and T_2^v vibrational normal modes do not effect the electronic E_g^e ground state or the acoustic modes containing only that i.r. The presence of the relaxation for the transverse mode of the E_g i.r. and absence for the mode of T_{2g} i.r.

is a direct observation of the low-level electronic + vibrational symmetry. A more complete description of the symmetry considerations for the stress wave in various lattices and interaction with defects will be considered elsewhere.

RELAXATION ATTENUATION PEAK SHAPE

The shape of the relaxation peak can be determined as a function of temperature through certain simplifying assumptions concerning the relaxation times of the scattering process. In particular, if only one relaxation mechanism of a single relaxation time is present and it is independent of temperature, the maximum in attenuation takes on a simple symmetric form when plotted as $1/T$. Using the relationship between the relaxation time and the temperature, the resonance scattering can be determined as a function of temperature with the aid of the Debye equations. The Debye equations were originally derived for the dielectric relaxation and relate the frequency of the stress wave (ν) to the relaxation time by

$$\alpha = \alpha_0 \, 2\nu\tau/(1+\nu^2\tau^2), \tag{2}$$

where α_0 is the maximum in attenuation. For the measurements of this investigation, the stress frequency is fixed and the relaxation time varies as function of temperature. This leads to a maximum in attenuation as a function of temperature when $\nu\tau(T)=1$. A comprehensive treatment of the connection of the frequency measurements to temperature measurements is treated in a series of articles by Nowick and Berry.[12]

Often, a single relaxation process is not the exclusive contributor to the attenuation and a distribution of relaxation times is present. This is reflected in the shape of the relaxation maximum in two distinct forms. The peak may be wider than that predicted by the Debye relations for a single relaxation time where the width (δT_0) at one-half the maximum is given by

$$\delta T_0 = \Delta/2.635k, \tag{3}$$

where Δ is the energy level separation and k is Boltzman's constant. A peak wider than that given by Eq. (3) may result for a single microscopic process which experiences different local strain fields and leads to a macroscopic distribution of relaxation times. The relaxation peak can still remain symmetric for certain common types of distribution times as shown by Nowick and Berry.[12]

Another manifestation of more than one relaxation time is an asymmetry appearing in the shape of the peak when plotted as $1/T$, as in Fig. 9. The relaxation maximum is for a transverse wave propagating along the [110] direction. The asymmetry of the peak can be resolved in this case by assuming two relaxation processes as indicated by the dashed curves. The parameters used to define the shape of the large peak are determined from two measurements at different frequencies which lead to two different temperatures for the relaxation maximum, as described in a previous section. These parameters give an energy level separation of 14.3 cm^{-1} (1.75 meV) and a prefactor τ_0 of 4×10^{-11} sec. The difference between large peak

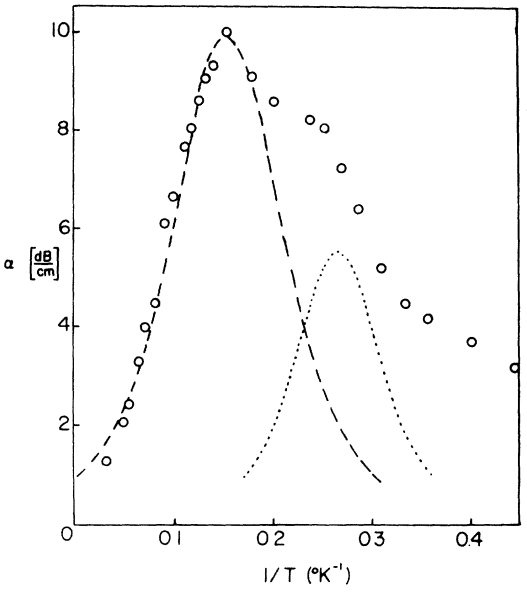

FIG. 9. Relaxation maximum of the attenuation shown in Fig. 7 plotted linearly and as a function of $1/T$. The dashed curves are calculated for two relaxation processes using tabulations of Ref. 12. The large-peak parameters ($\Delta_1=14$ cm^{-1} and $\tau_0=4\times10^{-11}$ sec) are deduced from the frequency-dependence measurements of Fig. 6 while the small-peak results ($\Delta_2=18.5$ cm^{-1} and $\tau_0=1\times10^{-12}$ sec) are obtained by curve fitting the difference between the large peak and the observed values.

TABLE V. Irreducible representations for a basis consisting of equivalent pure modes in a cubic lattice (O_h). The collection of i.r. (D) are labeled by the type of mode, propagation direction, and stiffness moduli.

Basis	Polarization	Irreducible representations
$D_L^{[100]}(c_{11})$		$A_{1g}+E_g$
$D_L^{[110]}(\frac{1}{2}[c_{11}+c_{12}+2c_{44}])$		$A_{1g}+E_g+T_{2g}$
$D_L^{[111]}(\frac{1}{3}[c_{11}+2c_{12}+4c_{44}])$		$A_{1g}+T_{2g}$
$D_T^{[100]}(c_{44})$	(100)	$T_{1g}+T_{2g}$
$D_T^{[110]}(c_{44})$	[100]	$T_{1g}+T_{2g}$
$D_T^{[110]}(\frac{1}{2}[c_{11}-c_{12}])$	$[1\bar{1}0]$	$A_{2g}+E_g+T_{1g}$
$D_T^{[111]}(\frac{1}{3}[c_{11}-c_{12}+c_{44}])$	[111]	$E_g+T_{1g}+T_{2g}$

and the measured attenuation is used to generate the smaller peak. The peak shape which best fits the residual attenuation results from an energy gap of 18 cm^{-1} (2.24 meV) and a prefactor of 10^{-12} sec. The sum of these two peaks reproduces the attenuation over much of the temperature range of interest. Since the parameters used to define the larger relaxation peak were determined independent of the peak shape, the less desirable procedure of curve fitting still yields useful information concerning the second peak. By varying the fitting parameters of the second peak, an estimate of the uncertainty in the determination of the energy level separation is ± 5%.

The foregoing procedure to reproduce the observed attenuation peak is not unique but only plausible. Another approach would be to assume an asymmetric distribution of relaxation times which could be used to reproduce the peak. Though this procedure would reproduce the observed peak, the relaxation distribution would provide little new physical insight due to the arbitrary width of the distribution. There is a natural prejudice for the simplicity of fitting the observed data with two peaks, since their physical interpretation is consistent with transitions between energy levels of a molecular cluster.

SPIN-ORBIT SPLITTING

The inclusion of the multiplicity of the E_g vibrational mode of the molecular cluster with the tenfold degenerate ${}^5E_g^e$ electronic ground state leads to ${}^5E_g$ and ${}^5A_{1g} + {}^5A_{2g}$ vibrational-electronic states. The anharmonic interaction stabilizes the Jahn-Teller distortion into either a tetragonal compression ($B > 0$) or an expansion ($B < 0$) of the cluster and removes the degeneracy of the first excited state with either the ${}^5A_{1g}$ ($B > 0$) or the ${}^5A_{2g}$ ($B < 0$) state lower. The choice of the sign of the anharmonic (and thus that of the Jahn-Teller distortion) component will be considered in detail later, but for clarity, the $B < 0$ will be adopted for the discussion of the spin-orbit interactions.

The spin-orbit splitting of the molecular cluster model has been calculated by Fletcher and Stevens.[2] Experimental parameters (δ tunneling splitting and D the spin-orbit interaction) used in the determination of the relative level separations of the energy levels are derived from APR g-factor measurements and an extensive investigation of the thermal conductivity of MgO containing transition metal impurities by Challis *et al.*[10] The g-factor is dependent on the ratio of δ/D. This ratio, as pointed out by Ham,[3] must be greater than one. The thermal conducitivity at low temperatures exhibited resonant scattering which was attributed to transitions between low-lying levels. Through plausibility arguments concerning the weighting and identification of various transitions, an energy level diagram was obtained and is shown in Fig. 10. The selection rule for transitions between the vibrational-electronic states, which are induced by vibrational excitations, is that the product of the i.r. of the initial and final states must contain the E_g^v i.r. This leads to two families of transitions between the A-E states and T states. The states which exhibit the largest matrix elements are shown in Fig. 9 connected by a solid line. The ordinate indicates the energy range of interest being ~ 30 cm^{-1} (3 meV [35 °K]).

The acoustic relaxation measurements were evaluated on the assumption of an indirect or Orbach process determining the rate. This is consistent with the most probable transitions for both the T and A-E family. The wavy line on the right- and left-hand sides indicates the level separations determined from the large and small relaxation maxima as outlined in a previous section. The magnitudes for the large peak agree rather well with the level separations for the T family. The thermal conductivity resonance scattering is also the largest for transitions involving the T family. The smaller peak does not lead to quite the same energy level as the A-E family (18 cm^{-1} compared

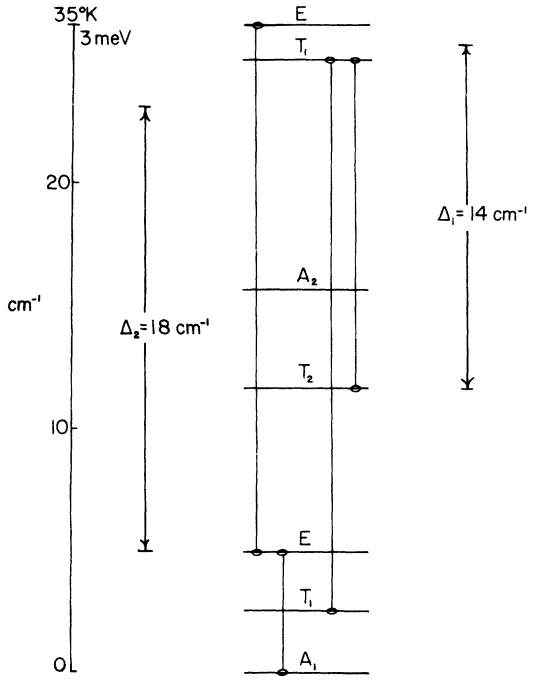

FIG. 10. Energy-level diagram including spin-orbit coupling constructed from Table 4, Ref. 10. The results of the relaxation measurements are indicated by Δ_2 and Δ_1 on each side of the diagram and are consistent with the $A \rightarrow E$ and T families of transitions. The lifetime broadening is estimated at less than 0.5 cm^{-1} from the determinations of τ_0.

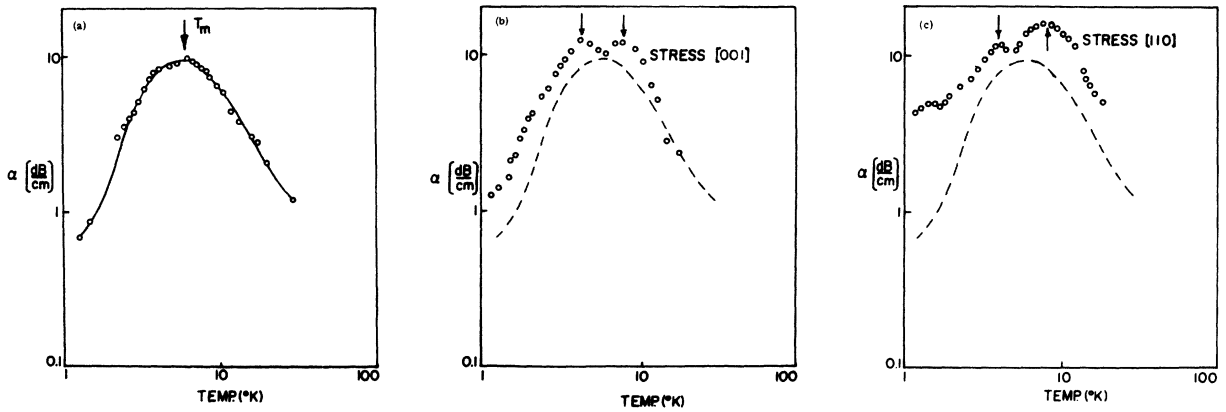

FIG. 11. Relaxation maximum for the slow-transverse mode propagating along the [110] axis in specimen No. 1 (1 GHz). Uniaxial strains of 2×10^{-4} is applied along the $[1\bar{1}0]$ and the [001] directions. The stress is calculated from the differential thermal expansion of a stainless-steel clamp fixed at room temperature and the MgO sample.

to a theoretical 22.3 cm^{-1}), but does approach it rather closely. The energy level diagram of Fig. 10 is calculated for a Jahn-Teller expansion of the lattice ($B<0$) and provides the best over-all fit to the spacings determined from the acoustic relaxation measurements. The expansion of the lattice site is plausible since the Cr^{2+} ion is most likely larger than the Mg^{2+} it replaces by analogy of the behavior of the Fe^{2+}, Fe^{3+} substitutional impurities.

A feature of the resonant scattering observed in the thermal conductivity, which is not seen in the hypersonic measurements, is the 5-cm^{-1} transitions associated with the $A_{1g}-E_g$ levels of Fig. 10. A hypersonic relaxation could occur due to this transition but at temperatures below the minimum measurement temperature (1.5 °K) according to Eq. (1) and assuming a measurement frequency of 1 GHz, a prefactor $\tau_0=10^{-11}$ sec (similar to the E_g-E_g transition), and a level separation of $\Delta=5$ cm^{-1}.

STRESS-INDUCED DEGENERACY REDUCTION

Application of uniaxial stress removes degeneracies in the energy levels through symmetry reduction of the molecular cluster. Transitions involving vibrational-electronic levels which have split due to the application of stress lead to a change in the acoustic relaxation phenomenon as shown in Fig. 11. The relaxation maximum is split into two distinctive peaks for stress applied either along the [001] or [110] directions. The positions of the maximum attenuations are approximately the same for either stress direction. Interpretation of the stress splitting is in terms of the large peak (considered in a previous section) which is associated with the T-family transitions.

The selection rules are modified for a reduction in the symmetry of the molecular cluster since the degeneracy in the E_g^v vibration mode can be removed. In particular, if the stress is assumed to

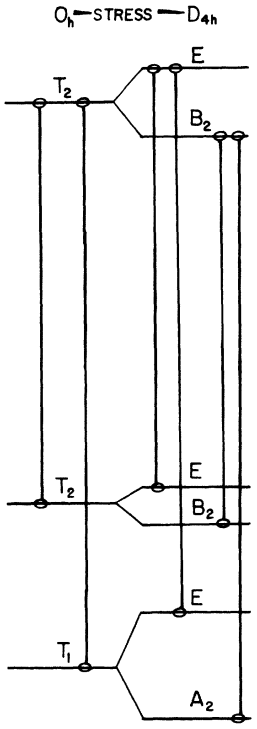

FIG. 12. Stress-split energy-level diagram assuming a reduction in symmetry from O_h to D_{4h} from Fig. 9. The transitions indicated are based on the selection rule for vibrationally induced transitions for D_{4h} symmetry which requires an A_{1g} or B_{1g} i.r. present. The separation of the energy levels is consistent with the magnitude of the peak splitting in Fig. 10 assuming τ_0 to be a constant.

reduce the symmetry from cubic (O_h) to tetragonal (D_{4h}), the E_g^v splits into an $A_{1g}^v + B_{1g}^v$ i.r. of the D_{4h} group. The selection rules for transitions between vibronic levels are modified so that the product of the i.r. of the initial and final states must contain an A_{1g} or B_{1g} i.r. to be induced by a lattice wave. The stress-induced splitting of the energy levels and the allowed transitions are shown in Fig. 12. If the relaxation maxima are viewed as being due to indirect transitions, the reduction in symmetry can lead to two groups of transitions which are analogous to the T-family transitions. These consist of E-family and A-B-family transitions of the D_{4h} group. Any further reduction of symmetry, for example to C_{2v}, offers more families of transitions than are observed.

The magnitude of the energy level separation of the split levels can be obtained using Eq. (1) and assuming the prefactor does not change. From this, the relative spacings of the members of the E and A-B families are estimated. A comparison of these values with the theoretical level separation as a function of strain due to Fletcher and Stevens is used to determine a value for the Jahn-Teller coupling coefficient. An estimate of strain leading to the peak separation of Fig. 10 is 2×10^{-4}. Fitting the split energy levels of Fletcher and Stevens[2] to the separations determined from the peak positions yields a Jahn-Teller coupling energy of 8.1×10^{13} cm^{-1}/m [1×10^{10} eV/m]. This is the same order of magnitude estimated by Fletcher and Stevens, but a factor of 2 smaller. It is also in agreement with Jahn-Teller energy calculated by Ham[3] using a point ion model.

CONCLUSIONS

The interaction of acoustic waves with strong coupling impurities offers a means of investigating the dynamic properties of the impurity systems. Symmetry determinations of the interaction of the ion with the lattice are possible through the use of various acoustic modes and polarizations. In the particular case of the chromous ion in MgO, only those acoustic waves that serve as a basis for the E_g i.r. interact through resonant scattering with the impurity system. This, in turn, reflects the selection rules derived from the symmetry of the mixed vibrational and electronic states of the molecular cluster.

Observation of relaxation absorption due to indirect transitions between vibrational-electronic states of the molecule, offers a means of quantitatively evaluating some of the parameters associated with the dynamic Jahn-Teller effect. In general, the experimental results indicate a tunneling splitting energy in the range of 14 cm^{-1} as assumed by Challis *et al.* Using an energy-level diagram of Fletcher and Stevens, assignments to particular families of transitions could be made. The high-temperature lifetimes associated with these families of states ranged from 10^{-11} to 10^{-12} sec.

The application of uniaxial stress split the relaxation maximum into two resolved peaks. By fitting the stress-split energy levels, assuming a D_{4h} symmetry to the theoretical results, a Jahn-Teller coupling energy of 8.1×10^{13} cm^{-1}/m is deduced. A value consistent with the Jahn-Teller energy as calculated from a point-ion approximation by Ham.[3]

ACKNOWLEDGMENTS

Discussion during the course of this investigation with E. Lafon, L. Halliburton, and W. Sibley contributed substantially to the progress of the work.

*Work supported by the National Science Foundation.

[1]C. A. Bates, J. M. Dixon, J. R. Fletcher, and K. W. H. Stevens, J. Phys. C **1**, 859 (1968).
[2]J. R. Fletcher and K. W. H. Stevens, J. Phys. C **2**, 444 (1969).
[3]F. S. Ham, Phys. Rev. B **4**, 3854 (1971).
[4]F. G. Marshall and V. W. Rampton, J. Phys. C **1**, 594 (1968).
[5]J. H. Van Vleck, J. Chem. Phys. **7**, 72 (1939).
[6]J. N. Lange, Phys. Rev. **176**, 1030 (1968).
[7]Material courtesy of Oak Ridge National Laboratory. M. Abraham, C. Butler, and Y. Chen, J. Chem. Phys. **55**, 3752 (1971).
[8]E. Sonder and W. A. Sibley, *Defects in Solids*, edited by J. H. Crawford and L. Slifkin (Plenum, New York, 1972), Chap. 4.
[9]R. Orbach, Proc. R. Soc. A **264**, 458 (1961).
[10]L. J. Challis, A. M. De Goer, K. Guckelsberger, and G. A. Slack, Proc. R. Soc. A **330**, 29 (1972).
[11]A. S. Nowick and W. R. Heller, Adv. Phys. **12**, 251 (1963).
[12]A. S. Nowick and B. S. Berry, IBM J. Res. Dev. **5**, 297 (1961).

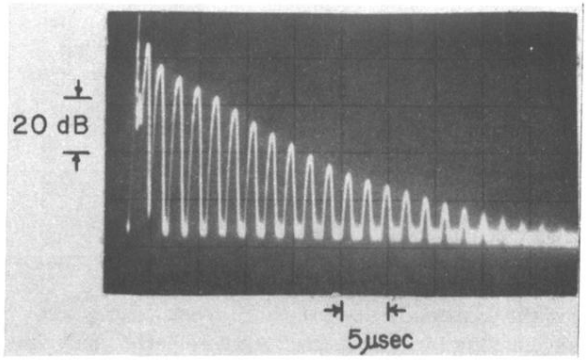

FIG. 3. Echo pattern for a longitudinal pulse which is multiply reflected between two parallel faces of sample No. 2. The pulse is propagating along the [100] direction at 77°K. Logarithmic amplification leads to the linear decrease in amplitude of the pulse envelopes. The carrier frequency (1 GHz) has been heterodyned and processed by a video detector.